Supplement of Atmos. Chem. Phys., 26, 6521–6539, 2026
https://doi.org/10.5194/acp-26-6521-2026-supplement

Atmospheric Chemistry and Physics
Open Access
EGU

Supplement of

Ventilation and low pollution enhancing new particle formation in Milan, Italy

Myriam Agrò et al.

Correspondence to: Myriam Agrò (myriam.agro@helsinki.fi) and Federico Bianchi (federico.bianchi@helsinki.fi)

Maps for the model simulation

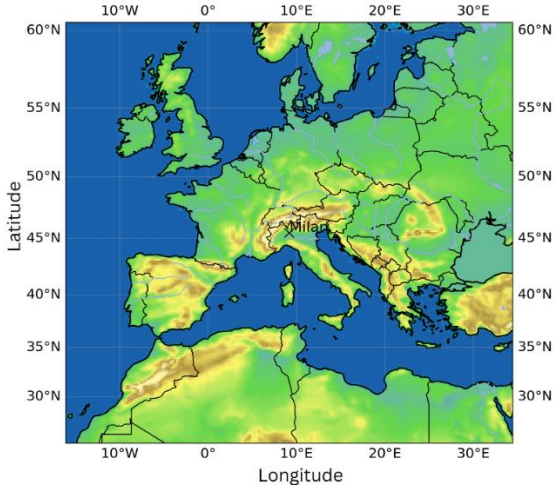

Figure S1: Domain for the WRF and FLEXPART simulation (spatial resolution of 18 × 18 km²).

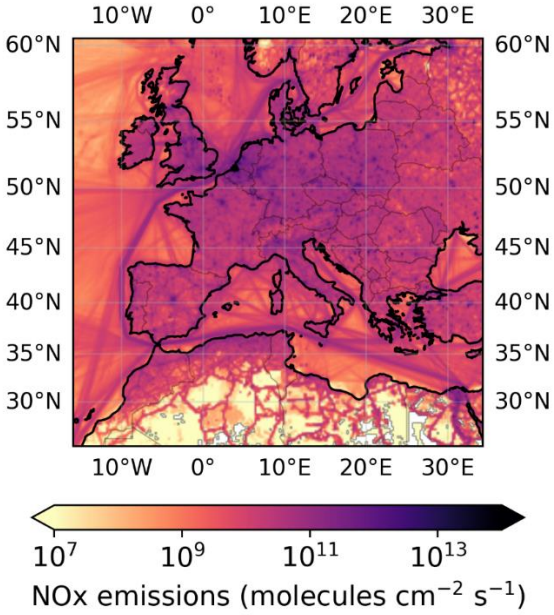

Figure S2: Map of NO_x emissions.

Discussion on the uncertainty of the growth and formation rates estimation

To assess the uncertainty associated with our method for the estimation of the growth and formation rates, we computed the GR for those days when a clear growth pattern was visible and when all the instruments were measuring simultaneously using the maximum concentration method (Kulmala et al., 2012). The number of days with these characteristics was 9 for the calculation of $GR_{3\text{-}7}$ and $GR_{7\text{-}20}$, and 7 for $GR_{20\text{-}100}$.

For clarity, in this discussion, the original method described in the article, and using the average size distributions of the days with NPF rank above the 80th percentile, is defined as **method 1.** The alternative method, consisting of the day-by-day estimation of the GR, is referred to as **method 2**. The GR and J calculated with the two approaches are reported in Fig. S3. Although $GR_{3\text{-}7}$ and $GR_{7\text{-}20}$ calculated with method 1 do not fall within the interquartile range of those calculated with method 2 (Fig. S3a), the limited amount of data points included in the boxplot could potentially create a bias in the comparison.

The J values obtained with the two methods remained very similar (Fig. S3b). A day-by-day comparison showed that the relative differences in the estimated J values were always below 10%, with the exception of four cases, which still remained below 21%.

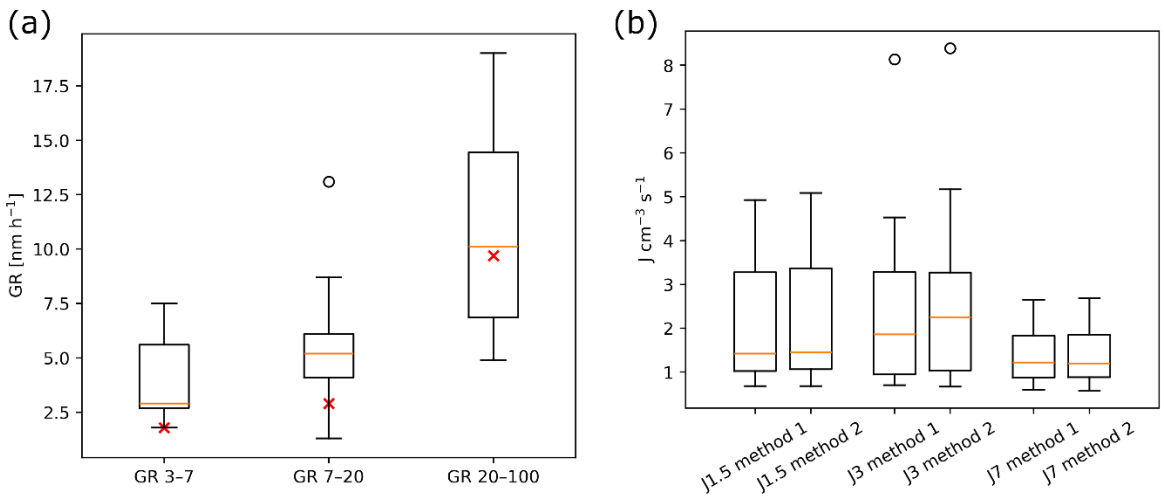

Figure S3: a) Boxplots representing the GR estimated using method 2, compared to the GR calculated using method 1 (in red x marks); b) comparison between formation rates calculated using the GR from method 1 and 2. The boxplots include only the days when the estimation of GR (and therefore J) with method 2 was possible. For the description of the boxplots, refer to Fig. 4b.

NPF analysis

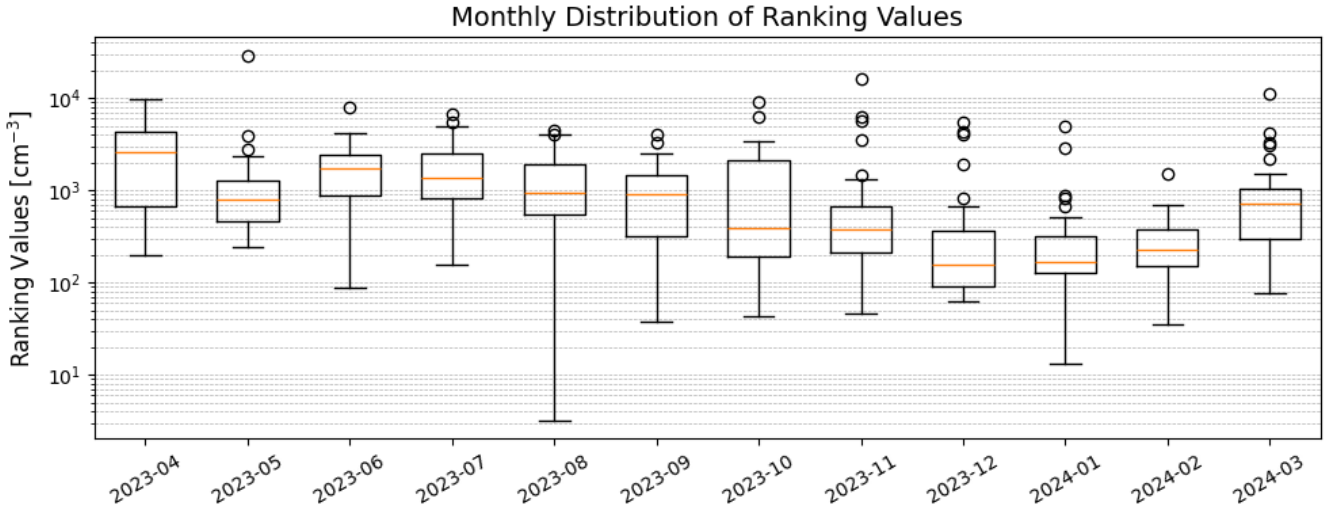

Figure S4: Monthly distribution of the ranking values. For the explanation of the boxplots, refer to Fig. 4b.

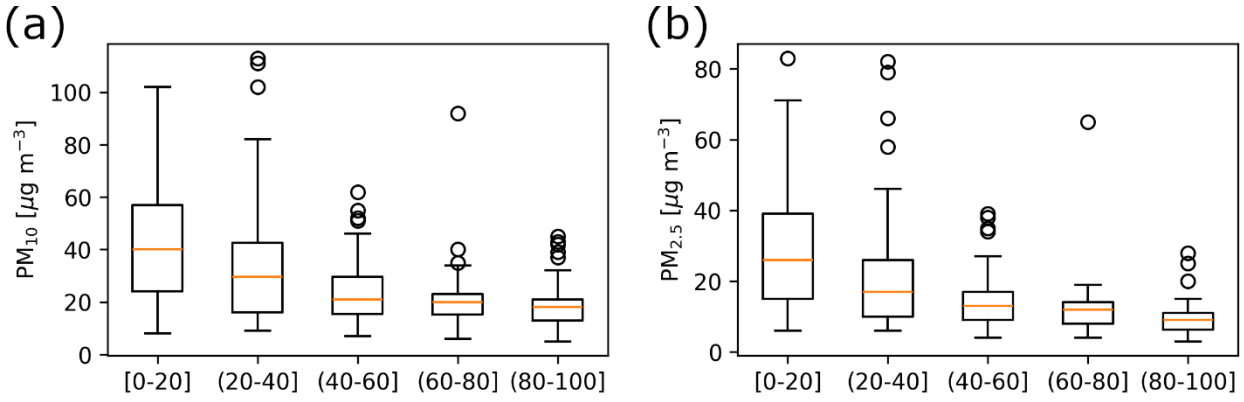

Figure S5: a) Daily PM_{10} and b) $PM_{2.5}$ per rank class. For the description of the boxplots, refer to Fig. 4b.

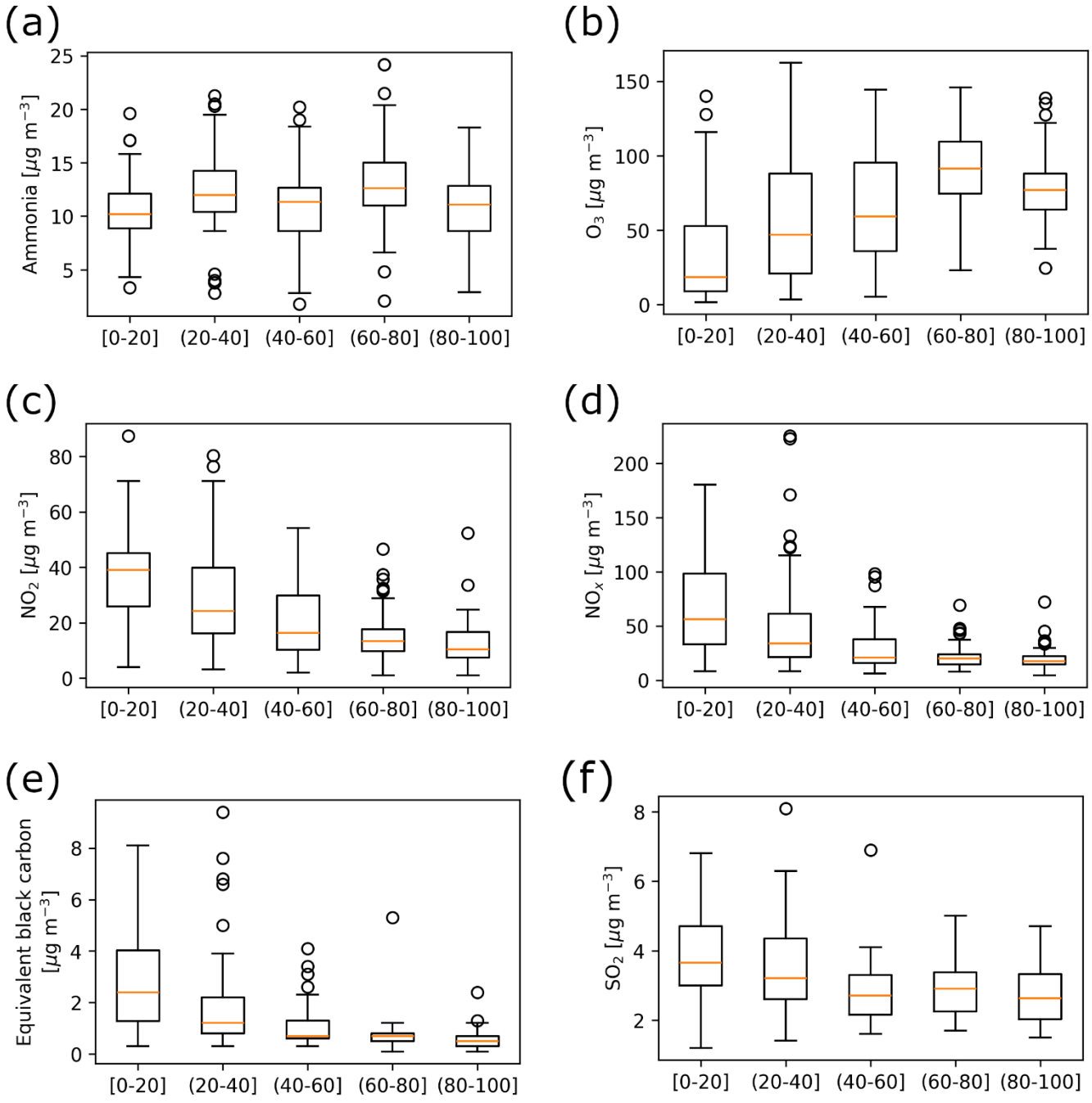

Figure S6: Daily median of a) ammonia, b) O_3, c) NO_2, d) NO_x, e) equivalent black carbon, and f) SO_2 concentration during the active window per rank class. For the explanation of the boxplots, refer to Fig. 4b.

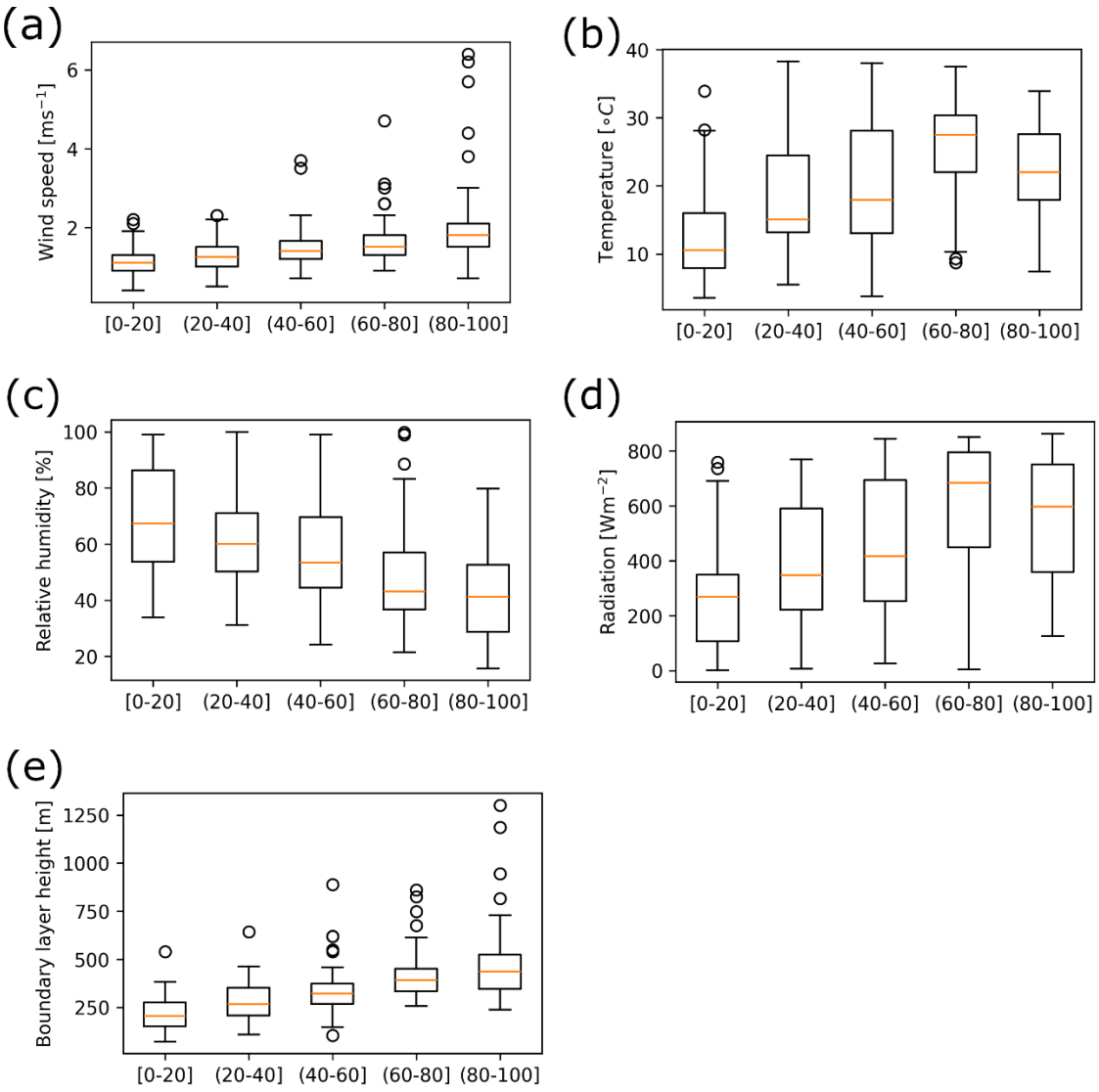

Figure S7: Daily median of a) wind speed, b) temperature, c) relative humidity, d) radiation, and e) boundary layer height during the active window per rank class. For the explanation of the boxplots, refer to Fig. 4b.

Sulfuric acid proxy analysis

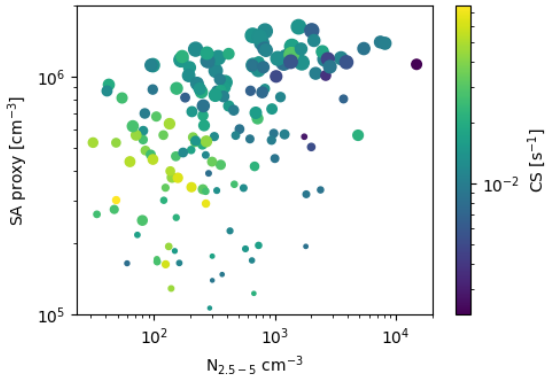

Figure S8: Relation between CS, sulfuric acid (SA) proxy, and $N_{2.5-5}$. The size of the dots represents the radiation. Each point corresponds to the daily median over the active time window.

NPF drivers in different atmospheric regimes

To assess the characteristics of the NPF drivers in different atmospheric regimes, the dataset was first separated into stagnant and non-stagnant days using the threshold set by ARPA Lombardia of VI=400 m^2 s^{-1}. Then the nano-particle ranking method was applied to each of the two subsets and the variables CS, formation rates, SO_2 concentration, and sulfuric acid proxy were analyzed in relation to NPF ranks. Finally, the full dataset was divided into seasons and the same analysis was performed.

The results obtained for the stagnant vs. non-stagnant analysis are reported in Fig. S9.

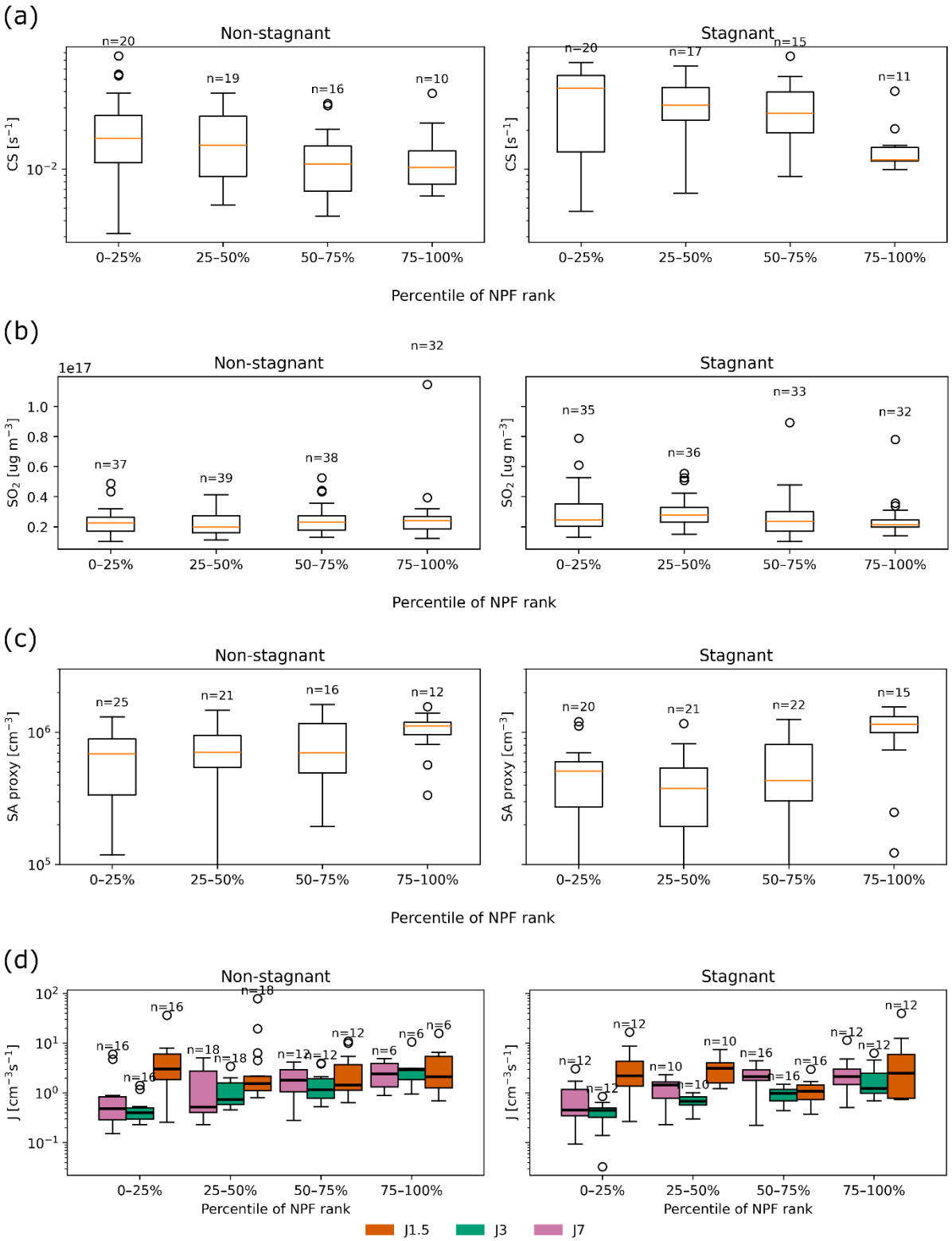
(a)
Non-stagnant
Stagnant
CS [s⁻¹]
n=20
n=19
n=16
n=10
n=20
n=17
n=15
n=11
0–25%
25–50%
50–75%
75–100%
Percentile of NPF rank
(b)
Non-stagnant
Stagnant
1e17
SO2 [ug m⁻³]
n=37
n=39
n=38
n=32
n=35
n=36
n=33
n=32
Percentile of NPF rank
(c)
Non-stagnant
Stagnant
SA proxy [cm⁻³]
n=25
n=21
n=16
n=12
n=20
n=21
n=22
n=15
Percentile of NPF rank
(d)
Non-stagnant
Stagnant
J [cm⁻³s⁻¹]
Percentile of NPF rank
J1.5
J3
J7

62

Figure S9: Daily a) median CS, b) median SO_2, c) median SA proxy calculated over the active time window of each day per rank class during stagnant and non-stagnant conditions; d) daily maximum $J_{1.5}$, J_3, and J_7 during the active window of each day, per rank class during stagnant and non-stagnant conditions. *n* indicates the number of datapoints included in the boxplot. For the description of the boxplot, see Fig. 4b.

The NPF intensities (concentration of 2.5-5 nm particles) were overall higher during non-stagnant conditions (Fig. S10):

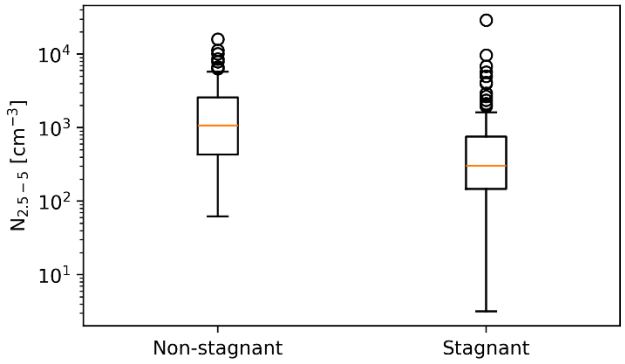

Figure S10: $N_{2.5\text{-}5}$, representing NPF intensity, as explained in Sect. 2.4.1, during stagnant and non-stagnant conditions. Boxplots are defined as in Fig. 4b.

Seasonal effects may further bias this analysis as stagnant days were recorded more frequently during autumn and winter, while non-stagnant days were more common in summer and spring (Tab. S1):

	Stagnant	Non-stagnant
Autumn	42	31
Spring	18	66
Summer	22	60
Winter	65	24

Table S1: Number of stagnant and non-stagnant days per season.

The results from the seasonal analysis are reported in Fig. S11:

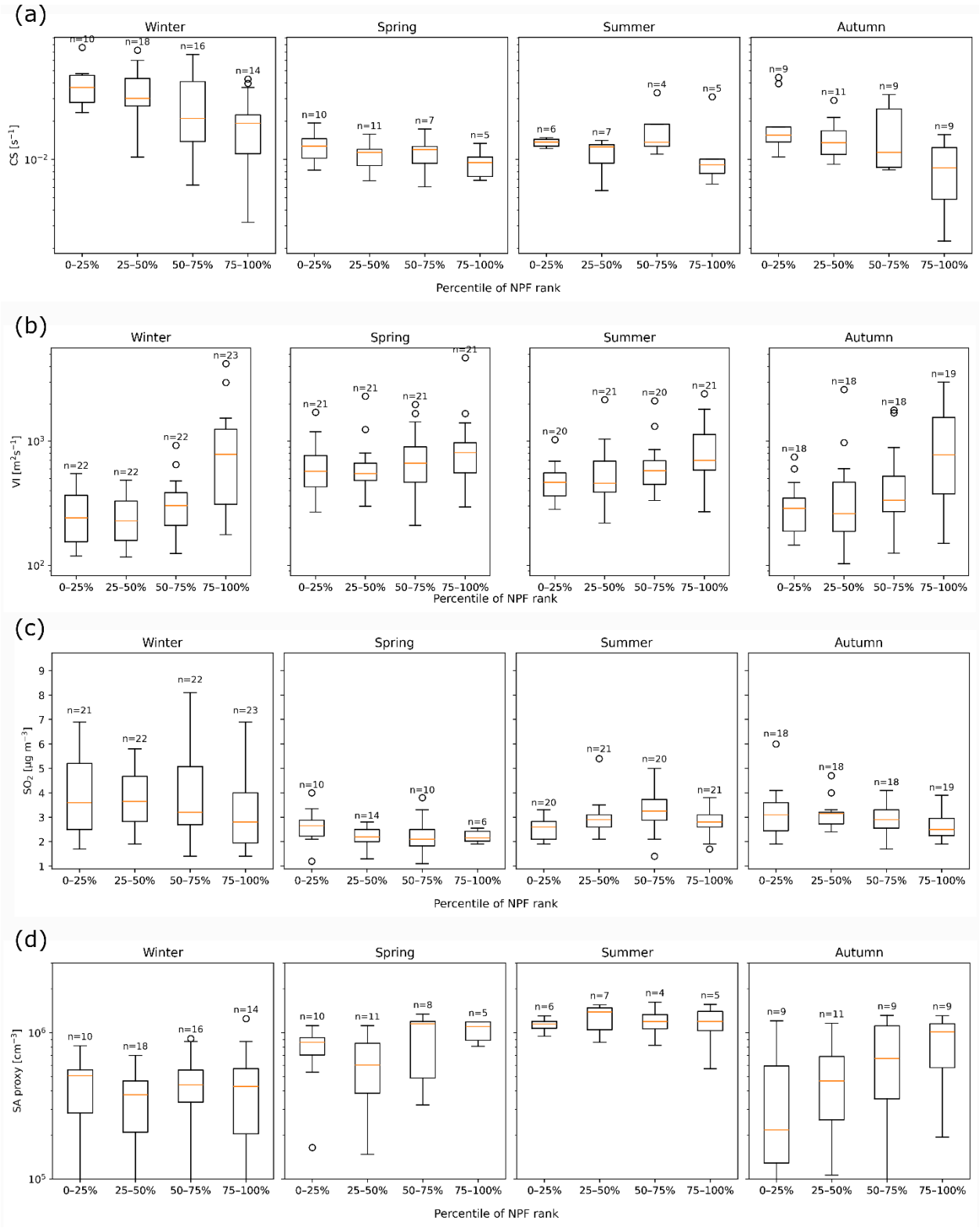
(a)
Winter
Spring
Summer
Autumn
CS [s⁻¹]
Percentile of NPF rank
(b)
VI [m²s⁻¹]
(c)
SO₂ [µg m⁻³]
(d)
SA proxy [cm⁻³]
0–25%
25–50%
50–75%
75–100%

78

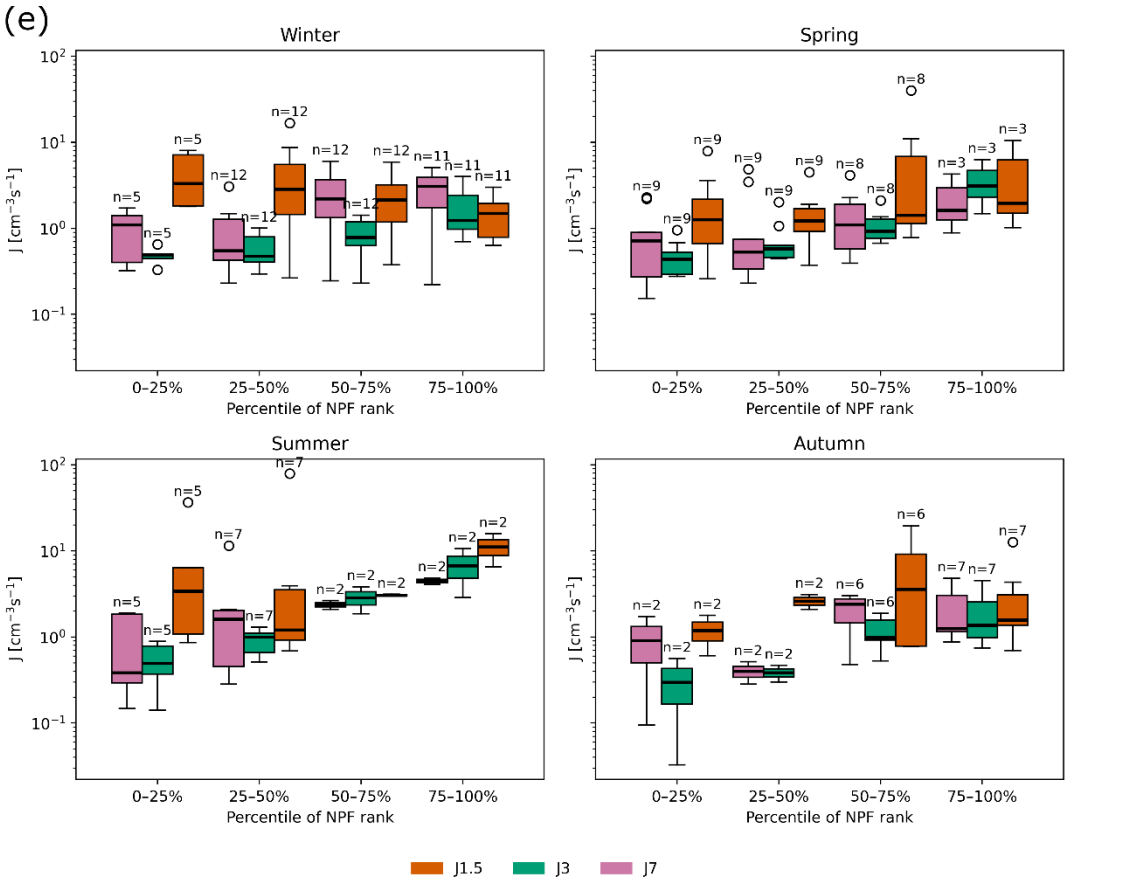
(e)
Winter
Spring
Summer
Autumn
J [cm⁻³s⁻¹]
0–25%
25–50%
50–75%
75–100%
Percentile of NPF rank
J1.5
J3
J7

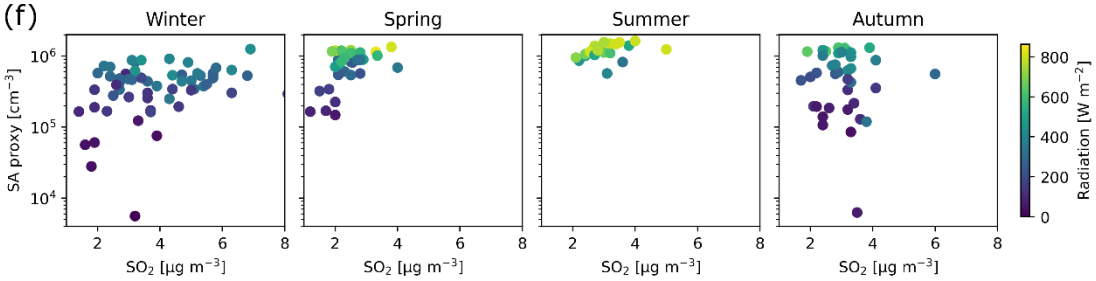
(f)
Winter
Spring
Summer
Autumn
SA proxy [cm⁻³]
SO₂ [μg m⁻³]
Radiation [W m⁻²]

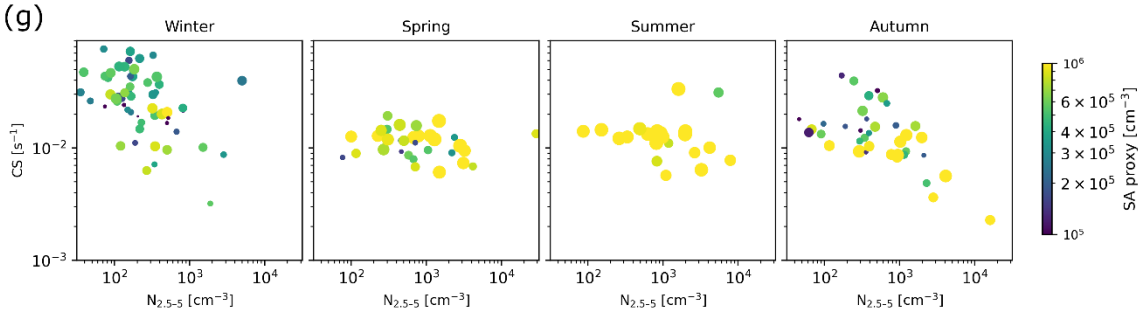
(g)
Winter
Spring
Summer
Autumn
CS [s⁻¹]
N2.5-5 [cm⁻³]
SA proxy [cm⁻³]

79

Figure S11: Daily a) median CS, c) median SO_2, d) median SA proxy calculated over the active time window of each day, per rank class in different seasons; b) daily VI per rank class in different seasons; e) daily maximum $J_{1.5}$, J_3, and J_7 during the active window of each day, per rank class in different seasons. *n* indicates the number of datapoints included in the boxplot. For the description of the boxplot, see Fig. 4b; f) relation between the daily median SA proxy, radiation, and SO_2 calculated over the active time window in different seasons; g) relation between the daily median CS, $N_{2.5\text{-}5}$, SA proxy, and radiation (size of the dots) calculated over the active time window in different seasons.